Internship report : Simulation of a laser link channel propagating through random medium

KOVALEVSKIJ Marcin Department of Physics, Université Paris Cité

1 Introduction

Propagation of light in the atmosphere is highly influenced by the weather conditions, such as rain, fog, snow, pollution and temperature fluctuations. These atmospheric phenomena influence optical wave phase, intensity and propagation path.

Atmospheric phenomena influence on properties of light can be grouped in three categories : **absorption**, **scattering** and **optical turbulence** (also known as fluctuation of index of refraction). Among these, absorption and scattering by gases and particles in the atmosphere depend on the wavelength and cause mainly *attenuation* of optical wave. Optical turbulence causes *intensity fluctuations*, *beam spreading* and *loss of spatial coherence*. As the consequence, random fluctuations of the index of refraction limits optical communications channel link bandwidth, and therefore its understanding is of a paramount importance in building FSOC (free space otpical communications) systems.

1.1 Internship goals

My initial internship goals were to study the effect of the turbulence on a optical beam propagating through random medium - atmosphere for a receiver (RX) at an orbital altitude of 700 km. However, during the internship goals of the simulation changed to also write a Graphical User Interface (GUI) that would facilitate future simulations.

1.2 Organization of the report

This report is organized into 5 chapters. In the chapters 2 and 3 I present the theory used to understand and model turbulence and its effect on a optical wave. In the chapter 4 I present my work accomplished during the internship and also the simulation results.

1.3 About the host organization

Astrolight is a Lithuania based start-up developing systems for ground-to-space optical communications. As stated on the official Astrolight website : "Astrolight's mission is to connect Earth and Space with high speed laser links, uncovering unprecedented capabilities for satellite connectivity and deep space exploration." [1]

2 Mathemathical models

In this chapter I present mathematical models of an electromagnetic field of a laser [2], I describe scalar diffraction theory, I introduce mathematical methods for modeling turbulence and finally I show how to propagate Gaussian beam through the atmosphere using scalar diffraction theory.

2.1 Modeling EM laser beam

I present here a mathematical model for describing complex amplitude of a single mode laser beam. A Gaussian beam is described as a paraxial wave. In its essence, a paraxial wave is constructed by taking a "carrier" plane wave, defined as $A\exp(-jkz)$ and forcing its complex amplitude A to slowly vary as function of wave displacement r, where $r = (x, y, z)$. We obtain a modulated complex wave, as function of r, of the following form : $U(r) = A(r)\exp(-jkz)$. Solution for

[1] https://astrolightspace.com/mission/

[2] Also known as a Gaussian beam.

$A(r)$ is then obtained by solving Helmholtz equation [3] $\nabla^2 U + k^2 U = 0$.

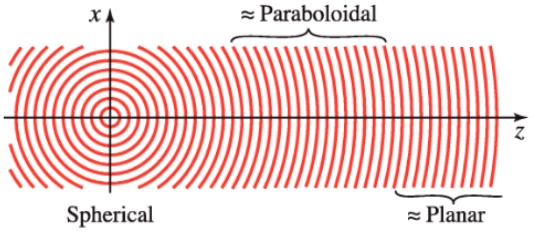

Figure 1: Variations of the spherical wave profile from the origin as function of distance z. At very far distances from the origin spherical wave can be approximated as a planar wave.([2], page 50.)

$$U(r,z) = A_0 \frac{w_0}{w(z)} \exp\left(\frac{-r^2}{w(z)^2}\right) \times \exp\left(-i\left[kz + k\frac{r^2}{2R(z)} - \psi(z)\right]\right) \quad (1)$$

where each term means:

- r is the radial distance from the optical axis
- z is the propagation distance
- $k = \frac{2\pi}{\lambda}$ is the wavenumber
- λ is the optical wavelength
- w_0 is the waist radius
- $w_z = w_0\sqrt{1 + \frac{z}{z_R}^2}$ is the beam waist
- $z_R = \frac{\pi w_0^2 n}{\lambda}$ is the Rayleigh range
- $\phi(z) = \arctan(z/z_R)$ is the Gouy phase

Optical intensity is then calculated as $I(r) = |U(r)|^2$ [4] and intensity at the center of the beam waist is given by $I_0 = \frac{2P_0}{\pi w_0^2}$ which allows to relate P_0 the total power of the beam with to beam intensity.

[3] For a complete derivation see [2] page 80

[4] The optical intensity is defined as the absolute value squared of the complex electric field.

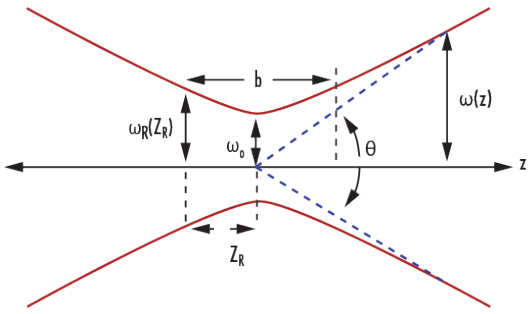

Figure 2: Most pertinent parameters of a Gaussian beam. (Taken from english Wikipedia, author DrBob, GFDL, see [12])

2.2 Scalar diffraction theory

In building FSO (free space optics) systems, it is common to encounter a problem where we're given a source-plane optical field $U(x_1, y_1)$ and we would like to know what is the resulting observation-plane field $U(x_2, y_2)$, at a distance Δz between two planes. The solution to this problem is given by Kirchhoff–Fresnel diffraction integral [5] presented below [6] :

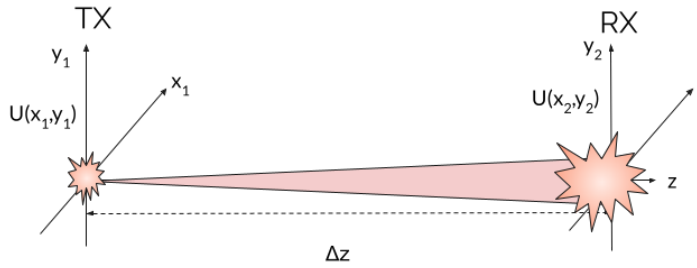

Figure 3: TX-RX axes in Cartesian coordinate system with corresponding optical field.

$$U(x_2, y_2) = \frac{e^{ik\Delta z}}{i\lambda\Delta z} \int\int U(x_1, y_1) e^{i\frac{k}{2\Delta z}\left[(x_1 - x_2)^2 + (y_1 - y_2)^2\right]} dx_1 dy_1 \quad (2)$$

An insightful observation is made by noticing that the equation (2) resembles double Fourier transform. Indeed, by careful expansion of square terms inside the exponential [7] the double integral can be re-written as the convolution of two functions :

[5] Derivation of this integral can be found in ch. 4 of ref. [2]

[6] the integration is defined over entire real space

[7] As demonstrated on page 86 ref [3]

$$U(x_2, y_2) = U(x_1, y_1) \otimes \left[\frac{e^{ik\Delta z}}{i\lambda \Delta z} e^{i\frac{k}{2\Delta z}(x_1^2 + y_1^2)} \right]. \quad (3)$$

The convolution theorem, which loosely speaking states, that convolution of two function g and h is equivalent to inverse Fourier transform of Fourier transforms G and H, $\{g \otimes h\}(x) = \mathcal{F}^{-1}\{G \cdot H\}$, allows to re-write the eq. [3] as a double Fourier transform.

2.3 Operator notation

Writing resulting equations for optical systems, as obtained by using Fresnel diffraction integrals, can quickly become "unreadable", therefore I introduce operator notation to facilitate writing of the resulting equations that follow. [8]

symbol	meaning
$\mathbf{r_1} = (x_1, y_1)$	TX coordinates
$\mathbf{r_2} = (x_2, y_2)$	RX coordinates
δ_1	grid spacing in TX plane
δ_2	grid spacing in RX plane
$\mathbf{f_1} = (f_{x1}, f_{y2})$	spatial frequency of TX plane
z_1	position of the TX plane on the optical axis
z_2	position of the RX plane on the optical axis
Δz	relative distance between TX and RX planes
m	scaling factor from TX to RX planes

We define the following operators :

$$\begin{aligned}
\mathcal{Q}[c, \mathbf{r}]\{U(\mathbf{r})\} &\equiv e^{i\frac{ik}{2}|\mathbf{r}|^2} \\
\mathcal{F}[\mathbf{r}, \mathbf{f}]\{U(\mathbf{r})\} &\equiv \int_{-\infty}^{+\infty} U(\mathbf{r}) e^{-i2\pi \mathbf{fr}} \mathbf{dr} \\
\mathcal{F}^{-1}[\mathbf{r}, \mathbf{f}]\{U(\mathbf{r})\} &\equiv \int_{-\infty}^{+\infty} U(\mathbf{r}) e^{i2\pi \mathbf{f} \cdot \mathbf{r}} \mathbf{dr} \\
\mathcal{R}[d, \mathbf{r_1}, \mathbf{r_2}]\{U(\mathbf{r_1})\} &\equiv \frac{1}{i\lambda d} \int_{-\infty}^{+\infty} U(\mathbf{r_1}) e^{i2\pi |\mathbf{r_2} - \mathbf{r_1}|^2} \mathbf{dr_1}
\end{aligned} \quad (4)$$

The parameters of an operator are given in the [] square brackets, while the operand is is in the curly {} braces.

[8] I borrow notation from [3] page 89.

2.4 Split-Step Beam Propagation algorithm

One of the methods to simulate optical wave propagation through random media is a *Split-Step beam propagation* method. The *Split* part in the name of the algorithm refers to the fact that the optical wave propagation is split into two parts. Mainly, it is considered that the beam propagating through space is split into the diffractive part due to the free space and refractive part due to the turbulence. Whereas *Step* part means that refractive and diffractive effects are calculated at a few defined points (steps) over the propagation distance.

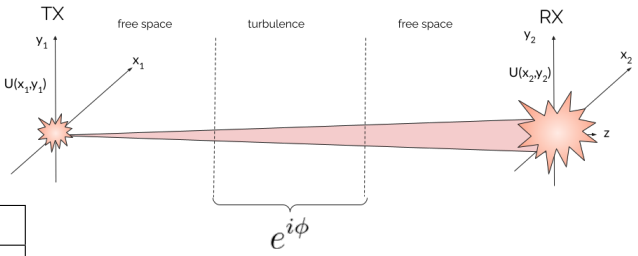

Figure 4: Split-step method idea.

In its most general form, a random medium refers to a medium which varies randomly and continuously in space and time. [**4**] In our case, the random medium is the atmosphere which is a linear, isotropic material with an index of refraction varying randomly in space, $n = n(x, y, z)$. When propagating field through N phase screens, for a small index of refraction n, such that, $\delta n = n - 1 \ll 1$, it can be shown that the field $U(\mathbf{r}_{i+1})$ in the $i+1$ plane of propagation can be written as :

$$\begin{aligned}
U(\mathbf{r}_{i+1}) \approx & \underbrace{\mathcal{R}\left[\frac{\Delta z_i}{2}, \mathbf{r}_i, \tilde{\mathbf{r}}_{i+1}\right]}_{\text{diffraction}} \times \\
& \underbrace{\mathcal{T}\left[z_i, z_{i+1}\right]}_{\text{refraction}} \mathcal{R}\left[\frac{\Delta z_i}{2}, \mathbf{r}_i, \tilde{\mathbf{r}}_{i+1}\right] \{U(\mathbf{r}_i)\}
\end{aligned} \quad (5)$$

Where $\mathcal{T}\left[z_i, z_{i+1}\right] = \exp\left[-i\phi(\mathbf{r}_{i+1})\right]$ is the operator representing the accumulation of phase, the method to generate $\phi(\mathbf{r}_{i+1})$ is introduced in the next chapter. While the $\tilde{\mathbf{r}}_{i+1}$ is a coordinate half-way in between i^{th} and $i^{th}+1$ planes.

Writing equation (5) in explicit manner yields :

Figure 5: Propagation path is sub-divided into N segments. (Inspired from [3] fig. 8.4).

$$U(\mathbf{r}_n) = \mathcal{Q}\left[\frac{m_{n-1}-1}{m_{n-1}\Delta z_{n-1}}, \mathbf{r_n}\right] \times \prod_{i=1}^{n-1}\left\{\mathcal{T}\left[z_i, z_{i+1}\right]\mathcal{F}^{-1}[\mathbf{f_i}, \frac{\mathbf{r}_{i+1}}{m_i}]\mathcal{Q}\left[\frac{4\pi^2}{k}\frac{-\Delta z_i}{m_i}, \mathbf{f_i}\right]\mathcal{F}[\mathbf{r_i}, \mathbf{f_i}]\right\} \times \left\{\mathcal{Q}\left[\frac{1-m_1}{\Delta z_1}, \mathbf{r_1}\right]\mathcal{T}\left[z_i, z_{i+1}\right]U(\mathbf{r}_1)\right\} \tag{6}$$

The eq. (6) can be implemented and computed with the help of Fourier transform libraries, for example, using Python3 programming language.

2.5 Random Fields & Theory of turbulence

Variations of temperature, pressure and wind speed induce changes in the refractive index. Changes in the refractive index alter optical properties of Earth's atmosphere and in turn cause distortions of optical waves propagating trough long atmospheric paths ([**3**] page 152). A good understanding of turbulence is necessary for all aspiring engineers working on systems concerned with propagation of optical waves via Earth's atmosphere, such as laser communications, adaptive optics corrections or laser weapons. In its essence, optical turbulence distorts intensity profile which results in intensity scintillation.

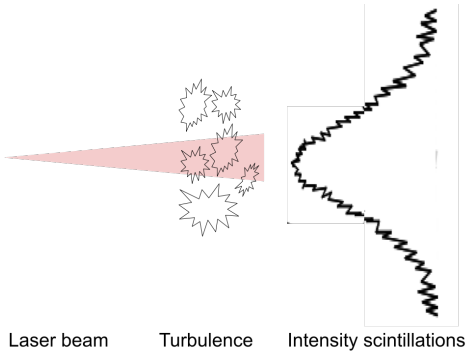

Figure 6: Intensity profile scintillations. Inspired from ([**1**], fig. 1.11)

The problem of modeling turbulence is the first principles physics problem of understanding how fluid changes velocity vector field. Such fluid problems are described by a general closed-loop non-linear coupled differential (Navier-Stokes) equations that are analytically tractable only for a handful of simple cases. To overcome this issue, the modern theory of turbulence was developed in 1940s by a Soviet scientist Andrey Kolmogorov who provided a statistical model to approximately describe (to a good degree) turbulence, as no closed-loop solution is possible.

Generally, from fluid mechanics side of view, a fluid flow can be separated into two categories : a laminar flow and a turbulent flow [9]. A fluid is said to be in a laminar flow when velocity profile of a fluid is uniform, while in the turbulent flow the fluid velocity changes drastically due to mixing of air at different temperatures, as the consequence the fluid acquires randomly distributed pockets of air, also called turbulent eddies.

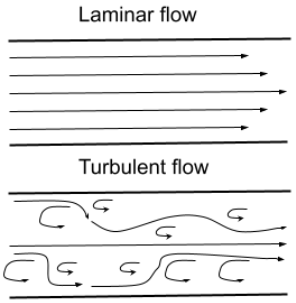

Figure 7: Laminar and turbulent flow profiles.

2.5.1 Structure functions

Kolmogrov proposed a theory in which he suggested that due to high wind velocities, such that the critical Reynolds number is exceeded (turbulent flow), formation of unstable air masses occurs (eddies). The formation of turbulent eddies allows for a transfer of energy from larger eddies, of the mean size L_0, to smaller eddies of the mean size l_0. In turn, the eddies of the sizes l, such that $l_0 < l < L_0$, form an inertial sub-range (figure 8).

In this sub-range, random fluctuations of a physical phenomena, here denoted as a random variable dependent on time $x(t)$ (e.g. wind velocity, temperature or refractive index) can be approximated as a process that depend on *stationary increments* $x(t + t_1) - x(t_1)$. Random functions

[9] The separation between the two modes of flow is made according to so called dimensionless Reynolds number

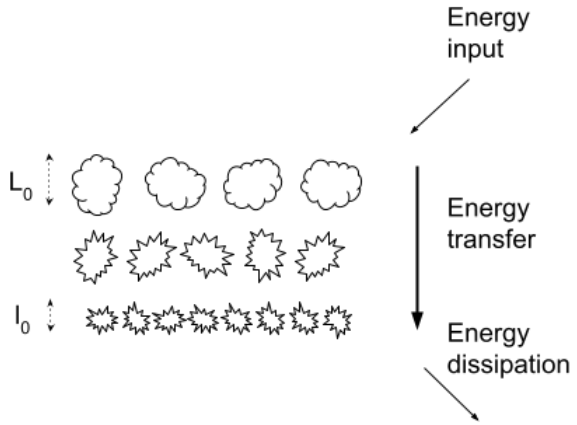

Figure 8: Kolmogorov theory of turbulence. Inspired by ([**3**] fig. 3.1.)

that can be approximated per stationary increments have a slowly varying mean and can be described in terms of *structure functions* instead of *covariance functions*. Then, such random process : $x(t) = \mu(t) + x_1(t)$ can be written as a sum of its mean value $\mu(t)$ and randomly fluctuating part $x_1(t)$, such that the mean of a fluctuating part $\langle x_1(t) \rangle = 0$. As the consequence, a structure function of a random process $x(t)$ is defined by :

$$\begin{aligned} D_x(t_1, t_2) &= \langle \big[x(t_1) - x(t_2)\big]^2 \rangle \\ &= \underbrace{\big[\mu(t_1) - \mu(t_2)\big]^2}_{\approx 0} + \langle \big[x_1(t_1) - x_1(t_2)\big]^2 \rangle \end{aligned} \quad (7)$$

[10]. The differences of two slowly varying means cancels out and structure function $D_x(t_1, t_2)$ reduces to the mean difference squared of fluctuating parts :

$$D_x(t_1, t_2) \approx \langle \big[x_1(t_1) - x_1(t_2)\big]^2 \rangle \quad (8)$$

The goal of introducing definition of a *structure function* above is to clarify the derivation of results that follow next.

2.5.2 Random fluctuations of refractive-index

When studying structure functions of random fields $x(t)$, index of refraction, wind velocity or temperature, a new parameter appear called structure constant C_x^2. For instance, in derivation of the structure function of the index-of-refraction $D_n(R)$ appears index-of-refraction structure constant C_n^2 (units $m^{-2/3}$), $D_n(R)$ is presented below:

$$D_n(R) = \begin{cases} C_n^2 l_0^{-4/3} R^2, & 0 \leq R \ll l_0 \\ C_n^2 R^{2/3}, & l_0 \ll R \ll L_0 \end{cases} \quad (9)$$

[10] [**4**] page 40.

,where R is the distance between two consecutive measurements and the refractive-index inner scale $l_0 = 7.4(\nu^3/\varepsilon)^{1/4}$ (m). Where ν is kinematic viscosity of a fluid (m^2/s^{-1}) and ε is average rate of dissipation of the turbulent energy per unit mass of a fluid ([**1**] page 59).

Physically, **the C_n^2 allows to infer about the variation of strength of the turbulence**. Variations of C_n^2 along the optical beam propagation path can be measured directly or indirectly inferred from the temperature structure constant C_T^2 (units $K^2 m^{-2/3}$), where P is the atmospheric pressure and in millibars and T is temperature in Kelvins and C_n^2 and C_T^2 are related as follows:

$$C_n^2 = \left(77.6 \times 10^{-6} \left(1 + 7.52 \times 10^{-3} \lambda^{-2}\right) \frac{P}{T^2}\right) C_T^2 \quad (10)$$

C_T^2 can be measured indirectly with the help of temperature structure function, for example, by measuring temperatures T_1 and T_2 with two wires at two different points, along the optical propagation path separated by a distance R between two measurements. Therefore, C_T^2 can be deduced by using temperature structure function:

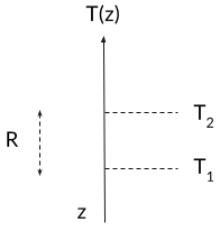

Figure 9: Measurement of C_n^2 from C_T^2.

$$D_T(R) = \langle \big[T_1 - T_2\big]^2 \rangle = \begin{cases} C_T^2 l_0^{-4/3} R^2, & 0 \leq R \ll l_0 \\ C_T^2 R^{2/3}, & l_0 \ll R \ll L_0 \end{cases} \quad (11)$$

, where the value of the inner scale l_0 for the temperature is proportional to the Kolmogorov length scale $l_0 = 5.8(D^3/\varepsilon)^{1/4}$ (m). Where D is the diffusion constant of air (m^2/s), and the outer scale $L_0 \sim \varepsilon^{1/2}$ (m) is directly proportional to the strength of the turbulence. Although the C_n^2 can be derived from C_T^2 measurements, it is possible to measure C_n^2 directly using a scientific instrument called a scintillometer.

Typical values of C_n^2 depend on atmospheric turbulence conditions and range from 10^{-17} $m^{-2/3}$ for weak turbulence up to 10^{-13} $m^{-2/3}$ for strong turbulence. For a beam of light propagating horizontally C_n^2 can be treated as constant, while

for a vertically tilted propagation path $C_n^2 \rightarrow C_n^2(z)$ depends from the propagation altitude z.

2.5.3 Power Spectral Density (PSD)

In physical and engineering sciences it is common that given a non-random (deterministic) function dependant on time $f(t)$ one may be interested in a frequency information contained in a function $f(t)$, then the function that provides frequency information of $f(t)$ is denoted as $F(\omega)$. According to the Fourier transform theory $f(t)$ and $F(\omega)$ are related as :

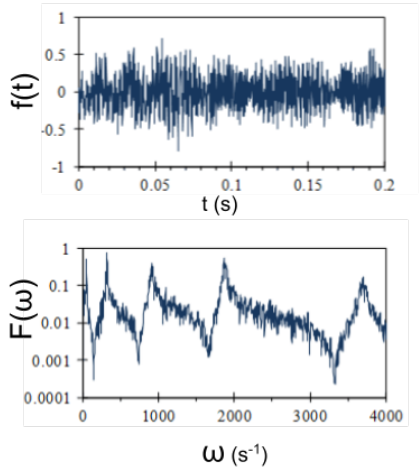

Figure 10: Fourier transformation of $f(t)$ allows to access to the $F(\omega)$, frequency information as seen by the frequency spikes on the $F(\omega)$, frequency information is otherwise hardly visible on $f(t)$.

$$F(\omega) = \frac{1}{2\pi}\int_{-\infty}^{+\infty} e^{-i\omega t} f(t)dt$$
$$f(t) = \int_{-\infty}^{+\infty} e^{i\omega t} F(\omega)d\omega \tag{12}$$

In analogous manner one may be interested in a spectral distribution (frequency information) of a function dependent on a random variable $x(t)$ or a random field $x(\mathbf{R}, t)$, where $\mathbf{R} = (\mathbf{x}, \mathbf{y}, \mathbf{z})$ is a space vector and t is time. In previous paragraph we introduced a structure function $D_x(R)$ which can depend on a random variable $x(t)$ or a random field. Correspondingly, it is possible to derive [11] a relationship between structure function (a random function) $D_x(R)$ and its spectral distribution $\Phi_x(\kappa)$, where $\kappa = 2\pi(f_x\hat{i} + f_y\hat{j})$ is angular spatial frequency in (rad/m) [12].

$$\Phi_x(\kappa) = \frac{1}{4\pi^2\kappa^2}\int_0^{+\infty} \frac{\sin\kappa R}{\kappa R}\frac{d}{dR}\left[R^2\frac{d}{dR}D_x(R)\right]dR \tag{13}$$

Calculation of the refractive-index power spectral density $\Phi_n(\kappa)$ using (eq.9) , yields :

$$\Phi_n(\kappa)^K = 0.033C_n^2\kappa^{-11/3} \quad \text{for } \tfrac{1}{L_0} \ll \kappa \ll \tfrac{1}{l_0} \tag{14}$$

, where super-index $\mathbf{K}$ in $\Phi_n(\kappa)^{\mathbf{K}}$ stands for Kolmogorov refractive-index power spectral density (PSD). However, because Kolmogorov PSD $\Phi_n(\kappa)^K$ is valid only over a narrow spatial band, mainly $\frac{1}{L_0} \ll \kappa \ll \frac{1}{l_0}$, other PSD were itnroduced, for example modified von Karman PSD (which is also used in random phase screen generation) is defined over $0 \leq \kappa \leq \infty$:

$$\Phi_n(\kappa)^{mvK} = 0.033C_n^2\frac{\exp(-\kappa^2/\kappa_m^2)}{(\kappa^2+\kappa_0^2)^{11/6}} \quad \text{for } 0 \leq \kappa \leq \infty \tag{15}$$

where $\kappa_m = 5.92/l_0$ and $\kappa_0 = 2\pi/L_0$ are respectively high-frequency and low-frequency modifications to the equation above. Also, when $l_0 \rightarrow 0$ and $L_0 \rightarrow \infty$, $\Phi_n(\kappa)^{mvK} \rightarrow \Phi_n(\kappa)^K$.

2.5.4 Fried parameter - $\mathbf{r}_0$

We have seen previously that turbulence strength is quantifiable via index-of-refraction structure constant $C_n^2(z)$. However, an intuitive understanding of $C_n^2(z)$ is somewhat tricky because of its units $(m^{-2/3})$. There are more intuitive quantities in describing atmospheric turbulence, one of them is r_0, having dimension of length and usually expressed in (cm).

Fried's parameter is also known as the *spatial coherence length* or simply *coherence diameter*. Fried's parameter r_0 is a scalar value derived from $C_n^2(z)$ integrated over the entire optical propagation path and formally defined for planar waves per equation below:

$$r_0(\lambda) = \left[0.423k^2\int_0^{+\infty} C_n^2(z)dz\right]^{-3/5} \tag{16}$$

When optical signal is propagating at an zenith angle ξ the atmospheric layer over which beam propagates increases by $1/cos\xi$, therefore r_0 changes to:

[11] For a detailed explanation please refer to [1] chapter 2.6.4

[12] [**3**] page 155

$$r_0(\lambda) = \left[\frac{0.423k^2}{cos\xi}\int_{\text{Vertical}} C_n^2(z)dz\right]^{-3/5} = (\cos\xi)^{3/5} r_0^{(vertical)}. \quad (17)$$

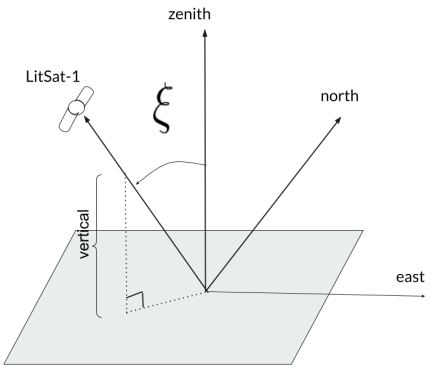

Figure 11: Optical beam traversing atmosphere at an angle ξ.

Loosely speaking, r_0 is a proxy quantity for estimating how "good" atmospheric conditions are at a given observation site. Strictly speaking, r_0 "indicates the spatial length over which optical wavefront can be considered as planar" (**[7]**). For more practical purposes, a rule of thumb is that the higher value of r_0 means better atmospheric conditions, for instance for $\lambda = 0.5\ \mu m$ we obtain $r_0 = 10\ cm$ which indicates a good observation site. [**7**].

From the equation above one can see that $r_0 \propto \lambda^{6/5}$ which show that r_0 is highly wavelength dependent. For instance, as it is mentioned in ([6] page 234) , $r_0(\lambda = 0.5\,\mu m) = 10\ cm$ and $r_0(\lambda = 20\ \mu m) = 8.4m$, this means that a telescope of a diameter of a few meters would be highly perturbed in the visible wavelength spectrum at $\lambda = 0.5\ \mu m$ and almost unperturbed in the IR spectrum range at $\lambda = 20\ \mu m$. It follows, that a better image resolution, for a given telescope diameter, is obtained in the IR than in the visible spectrum.

2.5.5 Numerical generation of random turbulent phase screens

In FSO simulations pipeline, numerically generated phase screens should approximate to a high degree real random process of which is the variations of the index-of-refraction. Because the variations of the atmospheric index of refraction are random therefore the optical propagation path is also random (**3**, p.166).

The goal of phase screen generation is to sample a 2D matrix of random phase values that satisfy statistics of the phase power spectral density, denoted in the following as $\Phi_\phi(\kappa)$. In previous paragraph we saw how to generate PSD (power spectral density) of a refractive-index random field, in the same manner, by using the phase structure function $D_\phi(r)$, of which definition is omitted here but can be consulted at ([**3**]), it is possible to show that for plane waves and weak turbulence, phase power spectral density is given by:

$$\Phi_\phi(\kappa) = 2\pi^2 k^2 \Delta z \Phi_n(\kappa) \quad (18)$$

the equation above can be directly expressed as a function of r_0, applying it to the modified Von-Karman PSD we obtain :

$$\Phi_\phi(\kappa) = 0.49 r_0^{-5/3} \frac{\exp(-\kappa^2/\kappa_m^2)}{(\kappa^2 + \kappa_0^2)^{11/6}} \quad (19)$$

In order to numerically generate turbulent phase screens we make an assumption that phase $\phi(x, y)$ induced by the turbulence can be written in the spatial frequency domain with the help of 2D Fourier transform:

$$\phi(x,y) = \int_{-\infty}^{+\infty}\int_{-\infty}^{+\infty} \Phi(f_x, f_y) e^{i2\pi(f_x x + f_y y)} df_x df_y \quad (20)$$

Then by applying Parsevals theorem we can relate optical phase $\phi(x, y)$ with the power spectral density of the phase $\Phi_\phi(\kappa)$:

$$\int_{-\infty}^{+\infty}\int_{-\infty}^{+\infty} |\phi(x,y)|^2 dxdy = \int_{-\infty}^{+\infty}\int_{-\infty}^{+\infty} |\Phi_\phi(f_x, f_y)|^2 df_x df_y \quad (21)$$

In addition, the phase $\phi(x, y)$ induced by the turbulence can be expanded in terms of Fourier series, where $c_{n,m}$ are Fourier coefficients :

$$\phi(x,y) = \sum_{n=-\infty}^{+\infty}\sum_{m=-\infty}^{+\infty} c_{n,m} e^{i2\pi(f_{x_n} x + f_{y_m} y)} \quad (22)$$

, we can equate Fourier coefficients $c_{n,m}$ to the expected optical phase variation as follows:

$$\begin{aligned}\langle |c_{n,m}| \rangle^2 &= \Phi_\phi(f_{x_n}, f_{y_n}) \Delta f_{x_n} \Delta f_{y_n} \\ &= \Phi_\phi(f_{x_n}, f_{y_n}) \frac{1}{L_x L_y}\end{aligned} \quad (23)$$

,where $\Delta f_{x_n} = 1/L_x$ and $\Delta f_{y_n} = 1/L_y$ are spatial frequency spacings and $\langle .. \rangle$ brackets indicate ensemble mean.

We can also express the equation above numerically :

$$\sqrt{\langle |c_{n,m}| \rangle^2} = (\text{rand(N)} + \text{i*rand(N)}) \sqrt{\Phi_\phi(f_{x_n}, f_{y_n}) \frac{1}{L_x L_y}} \tag{24}$$

Where rand(N) is a function that draws N random numbers according to the Gaussian distribution of zero mean and unit variance using random number numerical generation techniques. In order to obtain a random phase screen we simply calculate the real part of the inverse Fourier transform of the Fourier coefficients :

$$\mathcal{R}\{IFFT[c_{n,m}]\} \tag{25}$$

in doing so, we obtain the following turbulent phase screens :

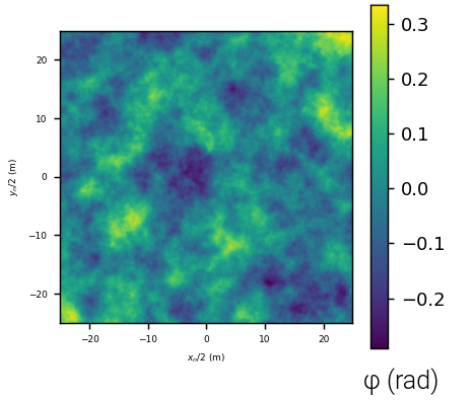

Figure 12: Generated phase screens using ft_phase_screen function from [3].

2.5.6 Phase screen movement in time

It is considered that the index-of-refraction in the atmosphere and hence turbulence varies over short, typically 100 μs periods of time. Because the optical waves propagate in the atmosphere with the speeds on the order of the speed of light 10^8 m/s, the time it takes for the turbulent eddies to change is negligible with respect to the time light takes to propagate through turbulent layers. As the consequence, it is considered that the physical phenomena that cause variations of the index of refraction in time, do not change by themselves, but vary because of the *advection* of these physical phenomena by mean wind velocity $\mathbf{v} = (v_x, v_y)$. In other words, static turbulence is "carried" in time across space by the wind. ([**3**] page 155). As such, this hypothesis allows us to introduce temporal dependence of phase more formally $\phi(x, y) \to \phi(x, y, t)$:

$$\phi(x, y, t) = \phi(x - v_x t, y - v_y t, 0). \tag{26}$$

The equation above allows to perform a dynamical FSO simulation by translating turbulent layers trough the atmosphere.

3 Simulation performance metrics

In the engineering of the FSO communication links, one can optimize for bit error rate minimization of the system, maximization of the received power, minimization of the scintillation index, minimization of the beam wander, or maximization of the strehl ratio. During this internship we have focused solely on the maximization of the received power and minimization of the scintillation index.

3.1 Maximization of received power

Our goal is to maximize received power both in time and space, denoted here as P_{RX}, which is simply integrated laser intensity over the aperture area and reads as :

$$P_{RX} = \int \int_{\mathbf{S}} |E(\mathbf{r})|^2 dS \tag{27}$$

,where S is the surface of the aperture.

3.2 Minimization of the scintillation index

Propagation of the laser signal through the atmosphere over great distances will lead to the intensity fluctuations in time. In designing FSO communications links the goal is to minimize such intensity fluctuations. Optical beam intensity fluctuations in time can be quantified with the help of a metric called the scintillation index, denoted as σ_I, it is defined as a normalized variance of the intensity :

$$\sigma_I = \frac{\text{var}[I]}{\langle I \rangle^2} = \frac{\langle I^2 \rangle - \langle I \rangle^2}{\langle I \rangle^2} = \frac{\langle I^2 \rangle}{\langle I \rangle^2} - 1 \tag{28}$$

[13]

We can see that if the beam intensity doesn't vary in time the second moment of the intensity becomes $\langle I^2 \rangle = \langle I \rangle \langle I \rangle = \langle I \rangle^2$ intensity mean squared, then for such ideal case, $\sigma_I = 0$. In other words, in FSO communications we would like to approach the ideal case as much as possible.

[13] Where the expression $\langle x^n \rangle$ indicates a statistical moment of the n^{th} order, $n = 1$ corresponds to the mean.

As one can see from the equation defining an electric field of a Gaussian beam, which is presented in the chapter (2.1), Gaussian beam intensity is stationary in time, which implies that $\sigma_I = 0$. We remark that we can employ this idea to verify the validity of the simulation results, in other words, with no turbulence (ideal Gaussian beam) we should obtain $\sigma_I = 0$.

4 Simulation

In the following section I describe how the simulation is written, how different pieces of the simulation fit together, and how the simulation results are validated theoretically.

The simulation is written in Python3 programming language with the help of open-source libraries, such as adaptive optics tools (Aotools [**12**]) and another adaptive optics library called (Soapy [**13**]) [which is the copyright Durham University and Andrew Reeves]. Also, immense credit deserves author Jason Daniel Schmidt for writing the book *Numerical simulation of optical wave propagation with examples in MATLAB* **[3]**. From *Schmidt's* book the main parts of physics algorithms were taken, such as: turbulence phase screen generation algorithm and split-step propagation algorithm.

From the software development point of view, the adaptive optics library - Soapy, written under the GPL-3.0 license, was repurposed from adaptive optics simulation tool for FSO communications simulations needs. Currently, the simulation and user guide can be find in the GitHub repository, under the following domain: https://github.com/MarcnKov/FSO-tool.

4.1 Putting it all together

The simulation is separated into five modules, as described on the diagram below. Mainly,

- *atmoshphere.py* handles turbulent phase screen generation and phase screen translation in time;
- *lineofsight.py* - propagates turbulent phase screens through the atmosphere [14];
- *helper.py* - module calculates miscellaneous quantities, such as intensity, and power at the receiver ;
- *simulation.py* - implements main simulation loop, handles exceptions, saving and coordinating data transfer in between modules;
- *gui.py* - implements graphical user interface and plotting;

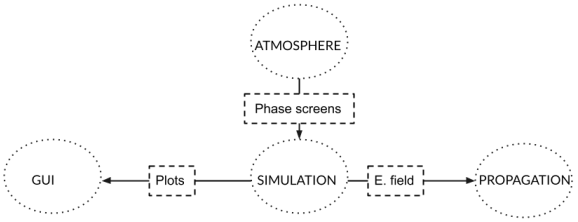

Figure 13: Simulation engine.

However, the bare-bone simulation could have been implemented simply by using code examples provided in the *Schmids* book by following the code flow diagram below. In such simulation we would firstly set-up simulation variables, such as grid spacing, optical beam type, beam power and other variables, then we would generate **n** turbulent phase-screens which we would propagate trough the atmosphere with the help of the split-step algorithm and finally we would calculate simulation metrics such as received power and scintillation index.

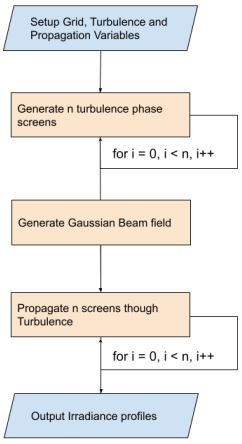

Figure 14: Basic implementation of a simulation.

4.2 Simulation sampling constraints

Numerical propagation of light trough free space requires computation of DFTs (discrete Fourier transforms). DFT as

[14] When there's no optical elements placed along the beam propagation path, TX can "see" RX, then it is called the line-of-sight propagation.

contrary to the continuous Fourier transform can cause aliasing because of discrete spatial domain sampling. [15]. In addition, a finite grid extent can cause energy spread beyond the boundaries of a grid which could result in ripples.([**3**, page 23])

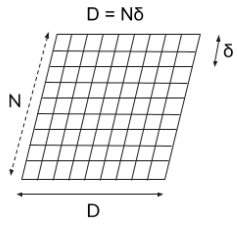

Figure 15: Finite extent of a simulation grid.

Theoretically, for a correct split-step propagation computation four inequalities have to be satisfied :

1. $\delta_n \leq \frac{\lambda \Delta z - D_2^{'} \delta_1}{D_1^{'}}$
2. $N \geq \frac{D_1^{'}}{2\delta_1} + \frac{D_2^{'}}{2\delta_n} + \frac{\lambda \Delta z}{2\delta_1 \delta_n}$
3. $(1 + \frac{\Delta z}{R})\delta_1 - \frac{\lambda \Delta z}{D1} \leq \delta_2 \leq (1 + \frac{\Delta z}{R})\delta_1 + \frac{\lambda \Delta z}{D_1}$
4. $N \geq \frac{\lambda \Delta z_{max}}{\delta_i \delta_n}$

Where the subscript n indicates n^{th} partial propagation screen (it could be a spatial extent of RX sensor) and a subscript i indicates i^{th} propagation screen (case $i = 1$ corresponds to the TX plane.) , such that : $1 \leq i \leq n$.
Other quantities are defined as follows :

- δ is a spatial grid spacing;
- $D_1^{'}$ and $D_2^{'}$ are TX and RX modified spatial extents;
- Δz is a total propagation distance;
- Δz_{max} is a maximum distance in between any two propagation planes;
- R is a wavefront radius of curvature;

The constraint (4) is the most limiting factor in simulations because many interesting applications, for example FSO communications, require large number of grid points because of the propagation distance. However, it is possible to overcome the constraint (4) by limiting the spread of the energy of the field over the boundaries by introducing absorbing boundary conditions and therefore reducing the number of grid points required for a simulation.

The absorbing boundary conditions prevent energy from the edges to creep into the center of the screen. For example, a Super-Gaussian function g_{sg} limits the spread of the electric field beyond the boundaries of a grid by filtering out electric field that creeps out beyond a limit, while not touching the energy in the center.

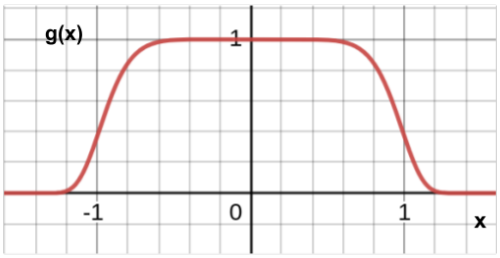

Figure 16: Super Gaussian absorbing boundary as defined per : $g_{sg} = exp\left[-\left(\frac{r}{\sigma}\right)^n\right], n > 2$ (n is not the number of partial propagations).

A single optical beam propagating through a random medium is otherwise equivalent to n partial propagations. Sub-division of a single propagation into n propagations is useful because it allows to attenuate the electric field across the propagation path in between turbulence layers, thus reducing the required N.

Division of a single propagation into multiple propagations allows to relax constraint (4) and swap it by a constraint that provides the information about the maximum Δz_{max} propagation distance that is possible in between two turbulent layers (in other words, it gives the maximum separation distance between two turbulent layers). Where δ_1 and δ_n corresponds to the TX and RX grid spacing.

$$4.\ \Delta z_{max} \leq \frac{min(\delta_1, \delta_n)^2 N}{\lambda} \tag{29}$$

By knowing the Δz_{max} it is possible to determine minimum partial propagations n needed for a total propagation distance Δz : $n = \lceil \frac{\Delta z}{\Delta z_{max}} \rceil + 1$.

The method for obtaining correct simulations results is as follows:

1. Determine N, δ_1 and δ_n from the constraints (1), (2) and (3);
2. Determine the maximum propagation distance in between two screens Δz_{max}, then calculate number of partial propagations n needed.

[15] Aliasing occurs when the spatial-frequency isn't sampled according to the Nyquist-Shannon sampling theorem, this causes spatial optical wave distortions

For example, we calculate the minimum constrains for a FSOC system defined by the following parameters : $\Delta z = 700km$, $\lambda = 1.55\ \mu m$, $D_1 = 0.5\ m$, $D_2 = 0.25\ m$, $\delta_1 = 0.02\ m$, accordingly we obtain the following inequalities on δ_2, N, Δz_{max} and n :

1. $\delta_2 \leq 2.16m$
2. $N \geq 1375$
3. $0 \leq \delta_2 \leq 2.19$ m

We choose $\delta_1 = \delta_2$, thus we obtain $\Delta z_{max} \leq 774\ km$, which implies $n = 2$.

We re-calculate the constraints with half of the previous grid-spacing by choosing $\delta_1 = 0.01\ m$, we obtain $N = 5462$ and $n = 5$.

When these constraints aren't satisfied we obtain the following artefacts:

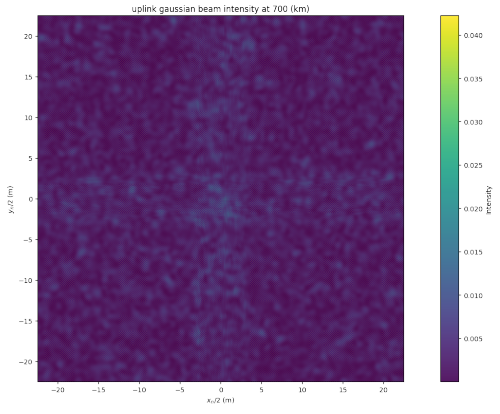

Figure 17: Cross artefact appears on the intensity image because of the under sampling issues. The solution is to decrease spatial domain frequency δ.

4.3 Simulation results

We begin the presentation of our simulation results by describing the simulation parameters:

- **Simulation:**
  - Number of grid points : 3000 (pixels)
  - grid size : 50 (m)
  - $\delta = \delta_1 = \delta_2 = 0.02$ (m)
  - number of iterations : 50
  - sampling rate Δ t : 1 (s)
- **Atmosphere:**
  - Number of turbulent screens : 10
  - Max turbulent screen height : 20 (km)
  - Average wind speed : 10 (m/s)
  - Average wind direction : 0 (deg)
  - r_0 : 0.14 (m)
  - l_0 : 0.01 (m)
  - L_0 : 20 (m)
- **Optical beam parameters:**
  - type : Gaussian TEM_{00}
  - beam waist w_0 : 17.5 (mm)
  - wavelength λ : 1.550 (μ m)
  - initial power P_{TX} : 10 (W)
  - propagation direction : up or down
- **Receiver:**
  - aperture diameter : 0.25 (m)
  - orbital altitude : 700 (km)
  - elevation angle : 90 (deg)

Below we present up-link and down-link simulation results of quantities of interest such as : intensity distribution at the receiver plane, collected power at the receiver aperture and scintillation index. Results are discussed and validated in the next section. All figures presented below indicate dynamic simulation results, i.e. the simulation where turbulence screens were translated in time at the sampling rate Δt.

4.4 Simulation validation

4.4.1 Orders of magnitude validation

We begin by performing simple sanity checks on our uplink simulation.

On the figure (18) we observe that the intensity field extends up to 20 m from one side, we know the analytical expression of the Gaussian beam waist $w(z)$ (given in the section 2.1), evaluating $w(700km)$ yields 19.73 m which seems to be in the range of expected value [total intensity field extension is obtained by calculating $2 \times w(700km)$].

We also calculate theoretical Gaussian beam intensity on the beam axis $I(r = 0, z = 700km) = I(0, z = 700km) = \frac{I_0}{1+(z/z_0)^2} = 0.016\ W/m^2$. On the figure (18) we observe that intensity ranges within analytical order of magnitude.

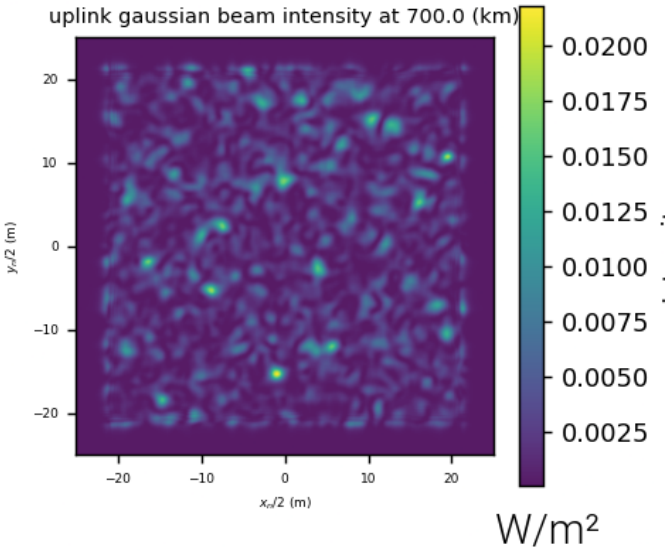

Figure 18: Uplink intensity distribution at RX.

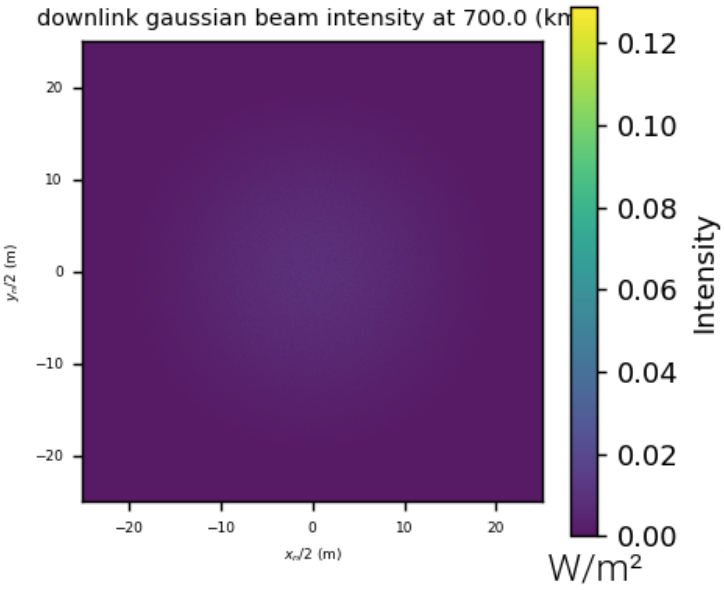

Figure 19: Downlink intensity distribution at RX.

On the figure (21) is represented the fluctuation of received power as function of time, calculating ensemble mean of received power gives us $P_{RX} = 0.6\,mW$. Also, from the peak intensity value $I(r = 0, z = 700km) = 0.016\,W/m^2$ we can calculate analytical received power as : $P_{RX} = I(r = 0, z = 700km)S_{aperture} = 0.016 \times \pi(0.25/2)^2 = 0.78\,mW$. Analytical and simulation results are within the same order of magnitude.

Atmospheric turbulence by itself does not cause direct

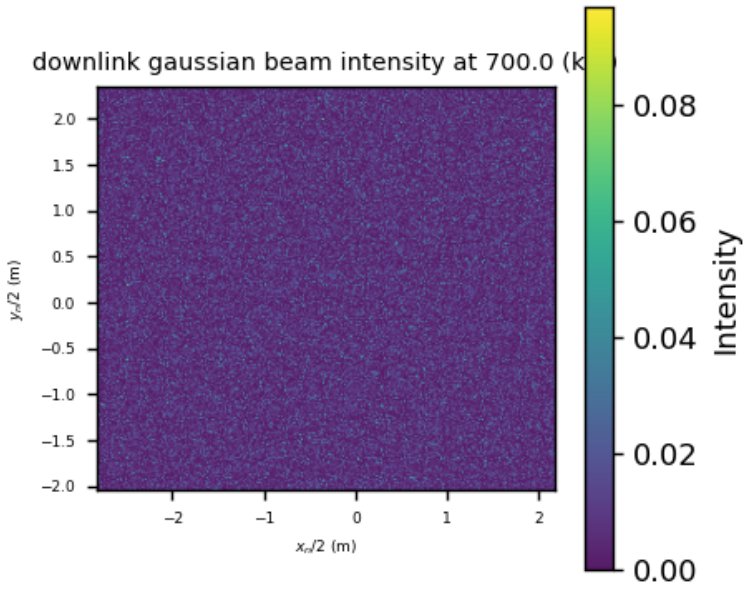

Figure 20: Downlink intensity distribution zoomed in W/m^2 at RX.

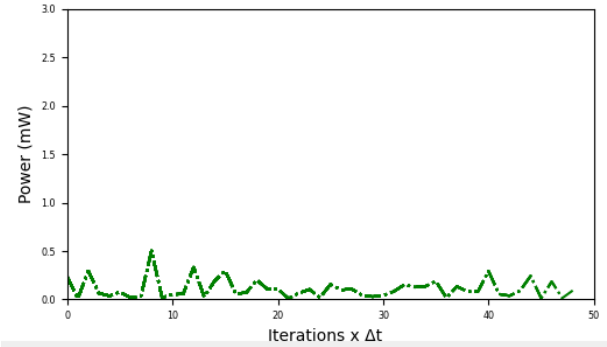

Figure 21: Uplink P_{RX} in W/m^2 at RX.

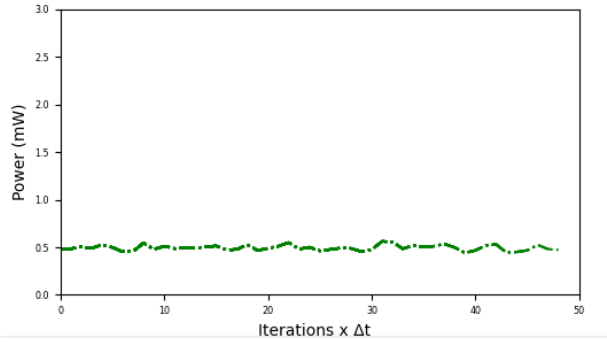

Figure 22: Downlink P_{RX} in W/m^2 at RX.

power loses along the optical beam propagation path, as absorption does. Instead, turbulence causes optical intensity random distribution transverse to the propagation path, which means that statistically less power will be collected at the receiver compared with non turbulent conditions. Be-

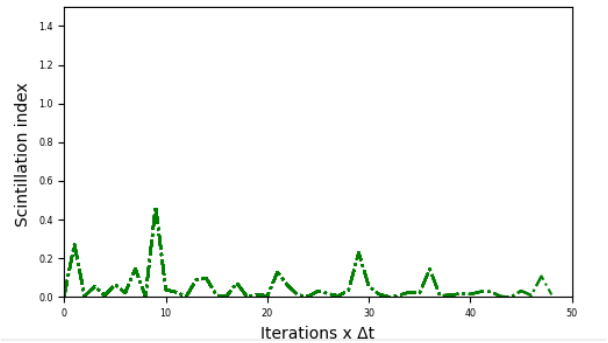

Figure 23: Uplink σ_I at RX.

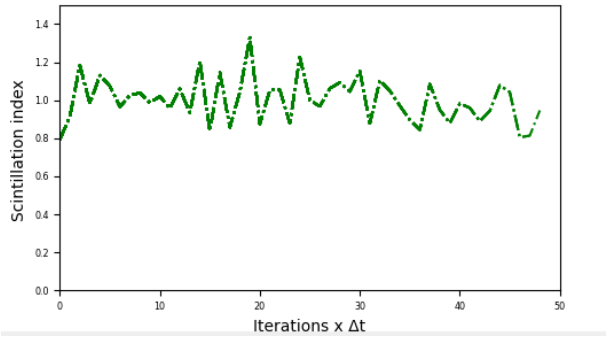

Figure 24: Downlink σ_I at RX.

cause we aren't modeling atmospheric absorbance, our system is closed, therefore the conservation of energy principle should be satisfied, mainly $P_{initial} = P_{final}$ initial energy should be equal to the final energy. Calculating $P_{total} = \Delta x \Delta y \sum\sum I(x, y)$, we obtain $P_{total} \neq 10W$, the conservation of energy principle is not verified because part of the energy that would spread is simply absorbed by absorbing boundaries. Repeating the simulation without energy absorbing boundaries we obtain $P_{initial} \approx P_{final}$. Energy conservation without absorbing boundaries can be used to estimate the validity of a simulation, ideally we should get $P_{initial} \approx P_{final}$.

Another simulation verification is performed by setting sampling rate $\Delta t = 0$, then the phase screen position $[\mathbf{x_{final}} = \mathbf{x_{initial}} + \mathbf{v} \times (\Delta t = 0)]$ should remain constant in time, and therefore metrics should be also constant. Accordingly, we obtain constant P_{RX} and $\sigma_I \approx 0$.

We can also switch off the turbulence by setting phase $\Phi(x, y) = 0$, such case is equivalent to propagate an ideal (as defined in 2.1) Gaussian beam trough the atmosphere up to the receiver. By switching off turbulence we obtain $\langle \sigma_I \rangle = 0$, which corresponds to the reasoning presented in the 3.2.

It is important to notice the differences between uplink and downlink intensity distribution results. Regarding the uplink image (18) we see the ripples on the edges of the screen, this indicates that the grid space is too small for the energy to expand correctly. Therefore, the simulation results could be still improved by increasing the screen size.

Regarding the downlink intensity simulation results, image (20), we can observe a complete pixelization of the intensity distribution. Such downlink simulation results indicate that the received light signal, if initially (at the TX) is perfectly coherent in space, after traversing through the Earth's atmoshpere spatial coherence is totally lost. This seems to be a highly unlikely result. The downlink beam intensity should be at least of the same distribution as the uplink. Mainly because, when the optical beam is traveling uplink, it encounters turbulent atmospheric layers at the first meters of the propagation, therefore the beam intensity spreads due to diffraction almost instantly. When the beam is travelling downlink it doesn't diffracts instantly because it propagates through the free space, diffraction free, almost the entire propagation path, until at the lower levels of the atmosphere it reaches turbulence layers. Downlink simulation results indicate that the algorithm used for downlink propagation is implemented incorrectly.

As it's indicated on the figures below fig. (25) and fig. (26), downlink images presented above are generated with the following (incorrect) algorithm - the ideal Gaussian beam is generated using eq. (1) for the distance (z = 680 km) up to the first turbulent layers, then it's propagated (with the split-step algorithm) through the atmosphere, up to the TX. The correct implementation of the downlink propagation algorithm should be simillar to that of the uplink propagation, mainly we would generate a Gaussian beam at the TX, then instantly we would propagate it using split-step algorithm up to the RX through the free space and turbulent layers.

After modifying the downlink propagation algorithm, I verify the simulations results by switching off turbulence and using the split-step algorithm to propagate the Gaussian beam trough free space with no diffraction. As one can see on the (fig. 27), the beam expands correctly and reaches peak intensity in the center of 0.016 W/m^2 (as predicted by theoretical results).

Further, I test the simulation algorithm for downlink static propagations by reducing the number of phase screens, increasing the grid spacing δ, switching off the absorbing boundary and changing turbulent phase screen heights (other parameters remain the same as previously), simulation pa-

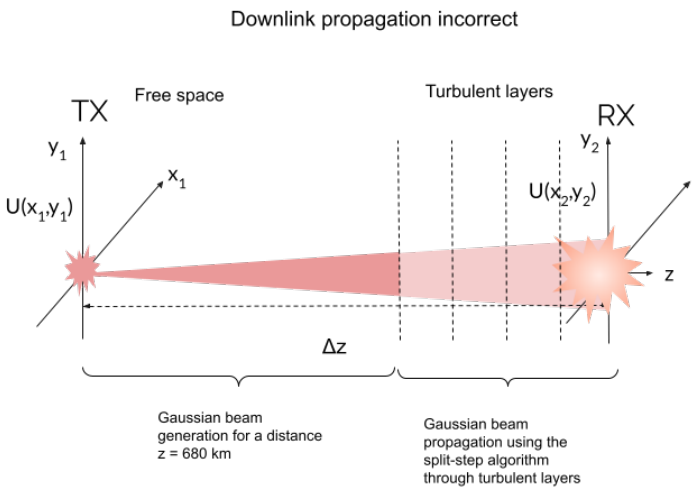

Figure 25: Incorrect implementation of the downlink proapgation algorithm.

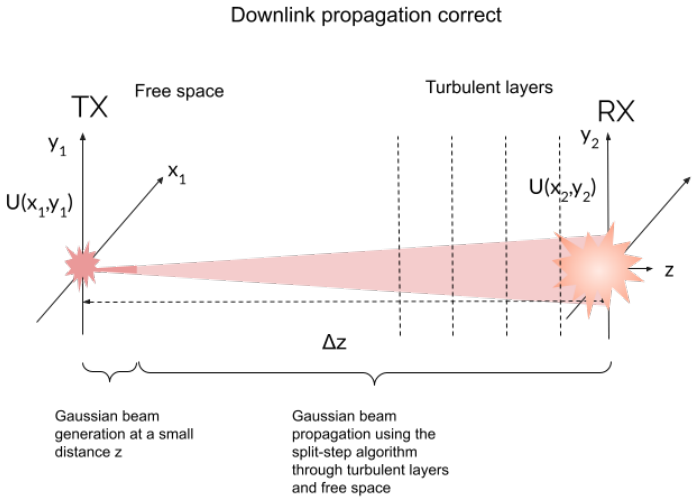

Figure 26: Correct downlink propagation using split-step method.

rameters for the intensities below are given under each figure, in the captions.

On the (fig. 28) we observe that placing phase screens close to the RX has almost no effect on distortion of the optical signal. When placing turbulent screens higher in the atmosphere as showed on the (fig. 29) intensity profiles become more pixelated.

By increasing the grid size even further, reducing the number of turbulent phase screens and switching off the absorbing boundary (other parameters remain the same as previously) we perform similar tests for the uplink case. On the figures (30, 31, 32, 33) one can observe that further we place phase screens from the TX, the free space propagation distance becomes greater and intensity distribution variation in-

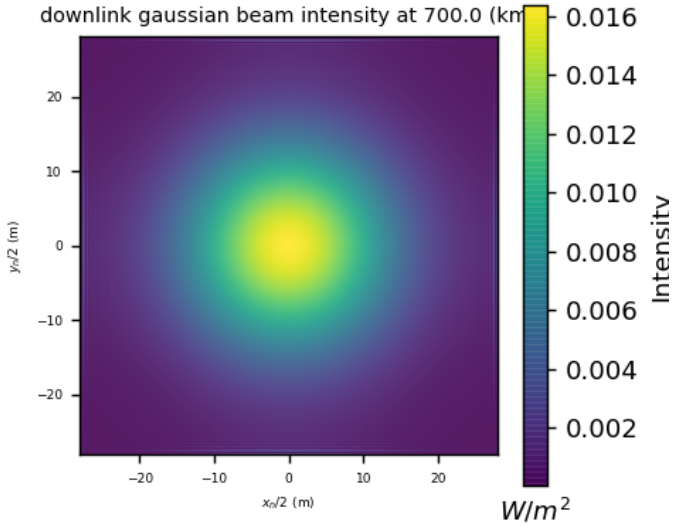

Figure 27: Correct implementation of the downlink proapgation algorithm using split-step.

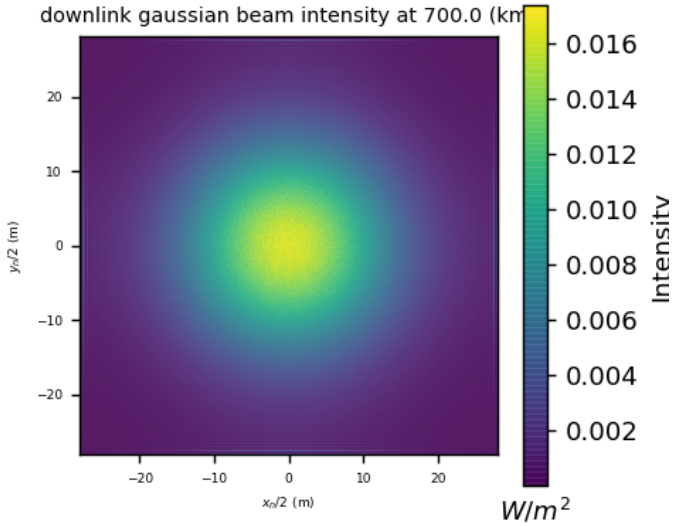

Figure 28: Downlink propagation, N = 3000, D = 56 m, turbulent screen heights : 10 m, 11m, 12 m.

creases.

We can also observe that uplink intensity profiles have a square shape and downlink intensity profiles have a round shape, even when Gaussian absorbing boundary is switched off for both uplink and downlink. We explain it as follows, for the downlink proapagation the otpical beam travels most of its distance through free-space unperturbed and only

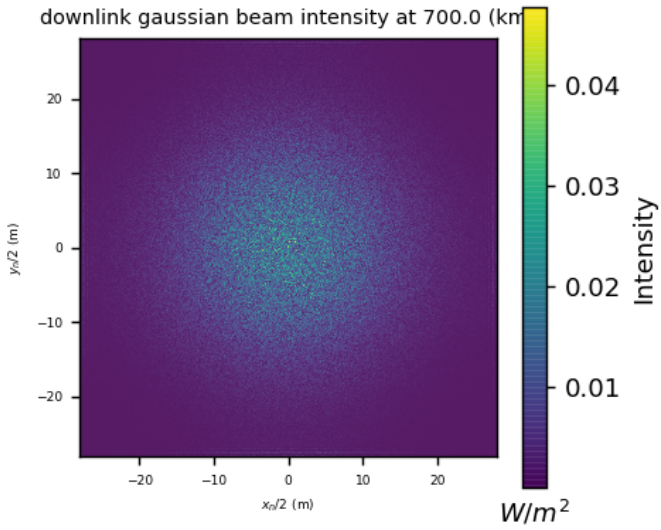

Figure 29: Downlink propagation, N = 3000, D = 56 m, turbulent screen heights : 10 m, 100m, 300m.

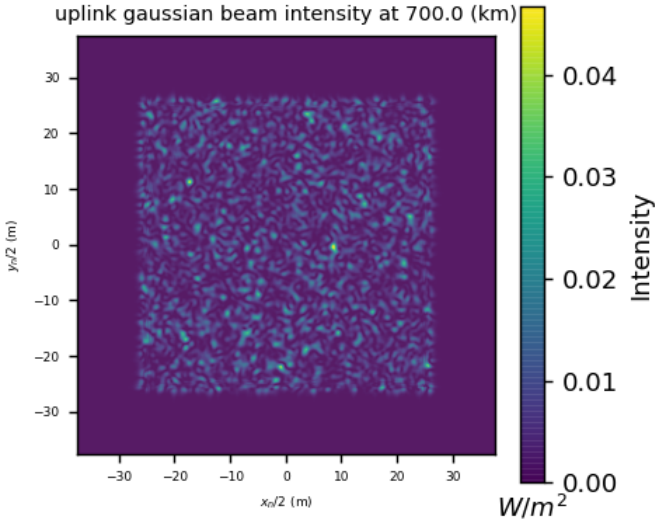

Figure 30: Uplink propagation, N = 3800, D = 75 m, turbulent screen heights : 10 km, 20 km.

reaches turbulent layers close to the ground (as explained before). Therefore, the split-step algorithm propagates almost entire optical beam with phase $\phi = 0$, while only close to the RX the optical beams encounters the turbulence and the optical signal is multiplied by the $n \times n$ square matrix containing phase values ϕ. Because split-step algorithm works by computing the inverse Fourier transforms, and inverse Fourier transform corresponds to a convolution, the optical beam acquires the shape of a square matrix. This effect is more notable in uplink propagations than downlink because in the uplink proapagation beam is immediately multiplied by the turbulent phase screens, as such it immediately acquires a square form.

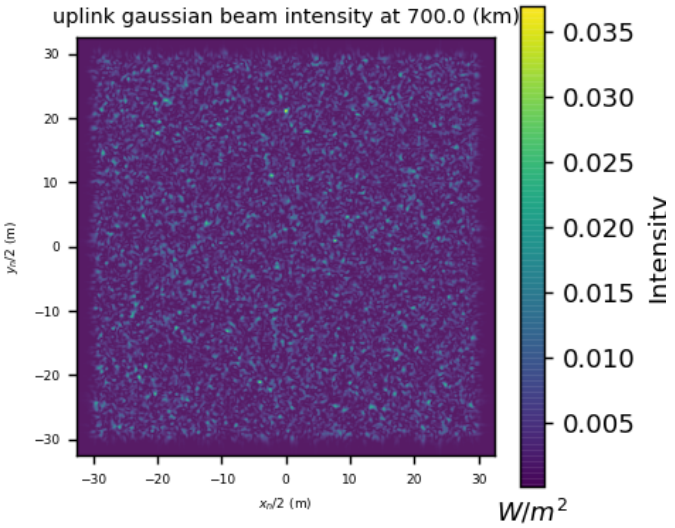

Figure 31: Uplink propagation, N = 3800, D = 75 m, turbulent screen heights : 35 km, 36 km.

4.4.2 Statistical validation

While order of magnitude verification can be a fair first order verification idea, the validity of a physical simulation emerges only while studying simulation ensemble statistics. A complete verification of the simulation would require to study ensemble statistics of the generated phase screens and propagated electric field both in static and dynamic cases.

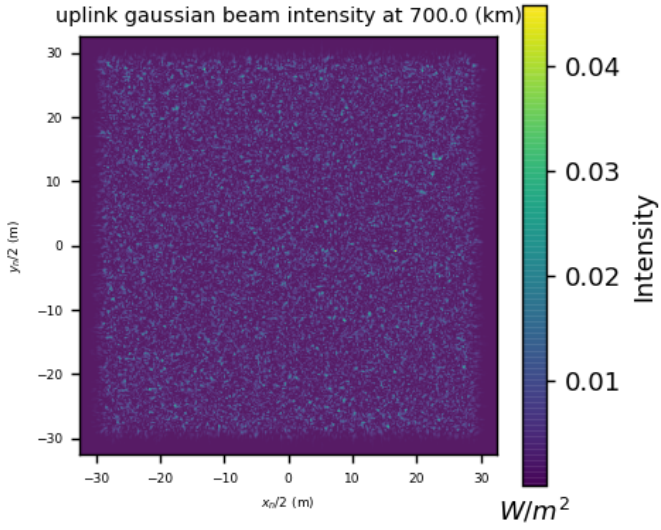

Figure 32: Uplink propagation, N = 3800, D = 75 m, turbulent screen heights : 50 km, 51 km.

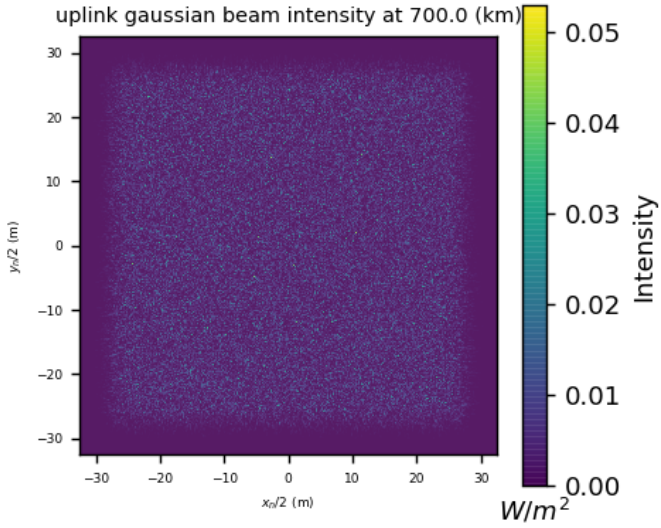

Figure 33: Uplink propagation, N = 3800, D = 75 m, turbulent screen heights : 100 km, 101 km.

In the following, I proceed to verify the propagated electric field in the static case. The verification of the static phase screens is omitted here, as such validation is already implemented in [**3**, page 180], for exactly the same algorithm as used in this simulation.

The main idea is to use independent and identically distributed random draws to calculate resultant statistical moments of random simulated physical variables, e.g. electric field, and compare them to analytically derived results.

I begin by verifying the propagation simulation results, for the static case, of the random optical field, defined here as $U(\mathbf{r}, z)$, where z is the propagation distance ([**1**] page 182).

For the simulation verification purposes, we're interested in calculating the second moment of the electric field $\Gamma_2(\mathbf{r_1}, \mathbf{r_2})$ - which is also known as the *mutual coherence function* (MCF) defined as :

$$\Gamma_2(\mathbf{r_1}, \mathbf{r_2}) = \langle U(\mathbf{r_1}, z) U^*(\mathbf{r_2}, z) \rangle \tag{30}$$

,where $U^*(r_2, z)$ indicates the complex conjugate of the electric field and $\mathbf{r_1}$ and $\mathbf{r_2}$ indicate the observation points at the RX plane and $\langle .. \rangle$ denotes the first moment or the ensemble average.

The MCF is used to determine the beam spreading caused by the turbulence, while also beam spreading can be caused by the diffraction. ([**1**] p.180)

When the observation points coincide $\mathbf{r_1} = \mathbf{r_2} = \mathbf{r}$, we obtain the *mean irradiance*:

$$\begin{aligned} \Gamma_2(\mathbf{r_1} = \mathbf{r}, \mathbf{r_2} = \mathbf{r}) &= \langle U(\mathbf{r}, z) U^*(\mathbf{r}, z) \rangle \\ &= \langle I(\mathbf{r}, z) \rangle \end{aligned} \tag{31}$$

and when $\mathbf{r_1} = \mathbf{r_2} = 0$ we obtain maximum mean beam irradiance.

Under the theory of weak fluctuations, for a plane-wave, the second statistical moment can be obtained by using Rytov theory ([**1**], p.183) : [16]

$$\Gamma_2(\rho, z) = \exp\left(-1.46 C_n^2 k^2 z \rho^{5/3}\right), \; l_0 \ll \rho \ll L_0 \tag{32}$$

, where ρ is the separation distance between two observation points in the RX plane.

We begin simulation verification results by setting new simulation variables:

- $\lambda = 1.55 \; \mu m$
- $C_n^2 = 10^{-14} m^{-2/3}$
- $N = 1000$
- $D_{RX} = 1m$
- $z = 21km$

[16] Plane-wave approximation is used here because for our simulation distances, 21 km, wavefront radius is basically planar.

- propagation direction - uplink

We accumulate the intensities of the electric field $I(\rho, z = 21\ km)$ for 40 iterations then we scale it by its on-axis value $I(\rho = 0, z = 21km)$, and finally we compute the scaled MCF $\Gamma_2(\rho, z = 21km)$ by varying ρ. [17] We plot the corresponding simulation results along with the theoretical ones on the figure below.

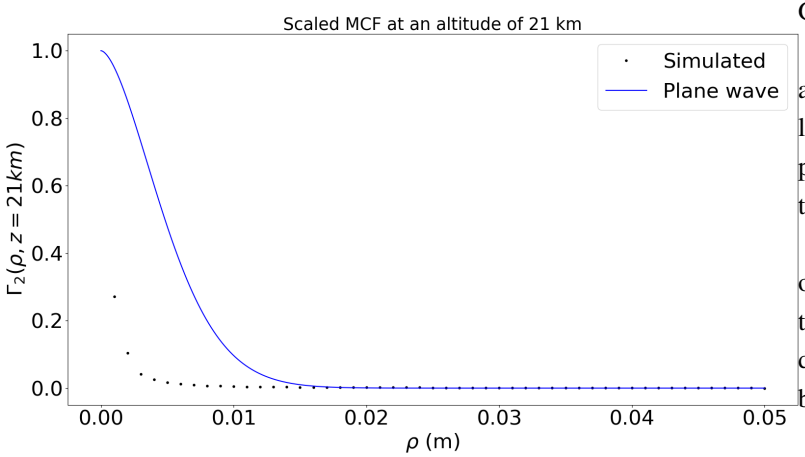

Figure 34: Comparison of simulated and theoretical scaled MCFs at an altitude of 21 km for uplink propagation.

We observe that the simulated results of the scaled MCF do not peak at 1 as the theoretical and the gap between two results is considerable. Currently, more time would be necessary to determine the cause of this discrepancy. Perhaps one could begin the troubleshooting by decreasing the grid spacing δ.

[17] A distance of 21 km was chosen instead of 700 km because of a limited computational power of my personal computer, the previous paragraph simulation tests at 700 km were performed on much more capable computational device located at the internship institution.

5 Conclusion

During this internship my main goal was to develop physics simulation to model Gaussian beam propagation through Earth's atmosphere. I consider that the main goal was accomplished as I developed a basic understanding on how optical wave propagation is modeled and I learned about a statistical theory of turbulence. Also, I re-purposed existing adaptive optics libraries for a development of a simulation engine and GUI to model free space optical communications link.

In addition, we saw that the choice of the simulation size and grid space is very important in obtaining correct simulation results. Also, we saw that the conservation of energy principle can be used to determine if the simulation parameters are well chosen.

Finally, I validated the simulation results with the order of magnitude estimations. However, the statistical validation yields the results that "resemble" theoretical ones, they do not match exactly, therefore additional simulation troubleshooting is necessary.

The simulation can be further studied by using more powerful computational devices, for example, one could further increase the grid size N and more turbulent screens can be placed on the signal propagation path. Then one could study the effects of such improvements on the statistical validation of the simulation.

Also, current simulation is implemented as a line-of-sight simulation, in other words, TX sees RX directly. In real FSO, the system isn't composed not only of the TX and RX but also of such optical elements as lenses, polarizers, filters and etc.., therefore, the simulation could be expanded by including models of such optical elements.

6 Credits

Firstly, I would like to credit Astrolight team:

- The CEO **Laurynas Mačiulis** and Program Manager **Vidmantas Tomkus** for providing this internship opportunity at Astrolight;
- The CTO **Dalius Petrulionis** for providing the support with the simulation scientific issues, for insights regarding simulation verification and initial internship report draft feedback;
- The Senior Engineer **Julijanas Želudevičius** for discussions regarding the validity of the simulation results and help with the simulation all along the internship;

- The Mechanical Engineer **Martynas Milaševičius** for useful discussions about FSOC links, support in the internship related issues and providing a welcoming internship environment;
- The Electronics Engineer **Andrius Stankevičius** for the discussions on how to build electrical optical detection systems;
- Other team members : **Laurynas Valčakas**, **Lukas Tamulevičius**, and **Ivan** for welcoming internship environment.

Secondly, I would like to credit scientific internship supervisor at my academic institution: Dr. Maria Amanti who works at "Laboratoire Matériaux et Phénomènes Quantiques" at the Université Paris Cité and who's reasearch topics spans:

- Integrated quantum photonics;
- Semiconductor sources of entangled photons;
- Novel techniques for quantum light characterization and manipulation;

for a scientific verification of my internship results.

Glossary

- **FSO** - free space optics;
- **FSOC** - free space optical communications;
- **TX** - signal transmitter;
- **RX** - signal receiver;
- **Uplink** - propagation of a signal up to the receiver, typically it is meant to be in the space;
- **Downlink** - propagation of a signal down to the receiver, typically it is meant to be in the Earth;

References

[1] Andrews, Larry C. *Laser beam propagation through random media* / Larry C. Andrews, Ronald L. Phillips.– 2nd ed., SPIE, 2005

[2] Bahaa E. A. Saleh & Malvin Carl Teich. *Fundamentals of Photonics, 2nd ed.* John Wiley & Sons. New York, 2007.

[3] Schmidt, Jason Daniel, *Numerical simulation of optical wave propagation with examples in MATLAB*, SPIE, Washington USA, 2010.

[4] BAOYONG LIU, *Optimal beam forming for laser beam propagation through random media*, Doctor of philosophy dissertation, Michigan Technological University, 2006. https://digitalcommons.mtu.edu/etds/78/

[5] Alan V. Oppenheim & George C. Verghese, *Signals, Systems & Inference*, Massachusetts Institute of Technology, USA, Pearson, 2016

[6] *L'observation en astrophysique*, Pierre Léna, Daniel Rouan, François Lebrun, François Mignard, Didier Pelat, EDP Sciences (2008), Edition CNRS, France

[7] PHY217 - *Observational Techniques for Astronomers* - online course, University of Sheffield, consulted 23/08/2022. PHY217

[8] *Statistics of a Geometric Representation of a Waveform Distortion*, D.L.Fried, Electro-Optical Labaratory, North American Aviation, Inc., Space and Information Systems Division, Torrance, California, February 1965

[9] Benjamin L. McGlamery , *"Restoration of turbulence-degraded images"* J. Opt. Soc. Am. 57(3), pp. 293-Ů297 (1967).

[10] Baoyong Liu *Optimal beam forming for laser beam propagation through random media, Michigan Technological University, Dissertation, 2006*

[11] Aotools - Adaptive optics tools library https://aotools.readthedocs.io/en/latest/introduction.html

[12] Montecarlo Adaptive Optics simulation, Andreew Reeves, 2014 https://soapy.readthedocs.io/en/latest/index.html